Structural, Optical, and Theoretical Studies of a Thermochromic Organic Crystal with Reversibly Variable Second Harmonic Generation

Michel Sliwa,[†,§] Arnaud Spangenberg,[†] Isabelle Malfant,[‡] Pascal G. Lacroix,[‡] Rémi Métivier,[†] Robert B. Pansu,[†] and Keitaro Nakatani*[,†]

PPSM, Institut d'Alembert, ENS Cachan, CNRS, UniverSud, 61 av du Président Wilson, F-94230 Cachan, France, and Laboratoire de Chimie de Coordination, CNRS, 205 route de Narbonne, F-31077 Toulouse Cedex, France

Received January 9, 2008. Revised Manuscript Received March 12, 2008

N-(3,5-Ditert-butylsalicylidene)-2-aminopyridine (**1**) exhibits bulk second harmonic generation (SHG) activity (2 vs urea). X-ray diffraction measurements show a non-centrosymmetric structure ($P3_2$). Experimental data of polarization-dependent SHG match the theoretical calculations on the basis of the crystallographic data. **1** is also thermochromic in the crystalline state, and SHG at 120 K is 4 times as high as at room temperature. Comparison is made with the isostructural isomer, *N*-(3,5-ditert-butylsalicylidene)-4-aminopyridine (**2**), which exhibits reversible photoinduced SHG variations.

Introduction

Nowadays, there is a strong need of devices in which properties can be reversibly changed upon an external trigger, such as light or heat. Variable transmittance lenses, memories, or actuators are among important fields of applications.[1] During recent decades, much attention focused on molecular materials. In fact, molecules' properties are (to some extent) predictable, and their design can be adapted according to the targeted properties. Moreover, if each molecule can be individually addressed, one information bit can be stored in a fraction of nm^3, and it would allow a considerable gain in terms of miniaturization of devices such as memories.[2]

A large number of *N*-salicylidene-anilines and *N*-salicylidene-aminopyridines, also known as Schiff bases or anils, undergo photochemically or thermally induced intramolecular enol−keto tautomerism (Scheme 1). Although this discovery dates back to the beginning of the XXth century,[3] the quite frequent and recent reviews testify to the continuous interest of the scientific community on this subject.[4] In fact, a reversible color change results from this reaction (photo- or thermochromism). Despite some exceptions,[5] the more stable form is the enol. In solution, tautomerism can only be photon-driven, and the keto isomer reverts back to the enol within a few milliseconds, and it can only be characterized by transient methods.[6] In the solid state, the keto isomer can be easily visualized upon UV irradiation or upon heating. Although a recent work demonstrates that photochromism

Scheme 1. Intramolecular Enol−keto Tautomerism in Anils. The Reaction Can Be Induced Thermally (Thermochromism) or Photochemically (Photochromism) And Leads, Respectively, To the Cis- Or Trans-Keto Isomer

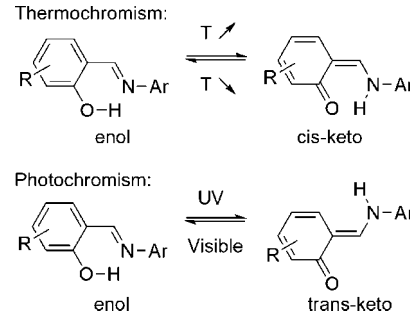

* To whom correspondence should be addressed. Tel. +33-1-4740-5594; fax +33-1-4740-2454; e-mail: nakatani@ppsm.ens-cachan.fr.
† PPSM, Institut d'Alembert, ENS Cachan, CNRS.
‡ Laboratoire de Chimie de Coordination, CNRS.
§ Present address: LASIR, UMR 8516, CNRS, Université des Sciences et Technologies de Lille, Bât C5, F-59655 Villeneuve d'Ascq Cedex, France.

(1) (a) Higgins, S. *Chim. Oggi-Chem. Today* **2003**, *21*, 63. (b) Winder, R. *Chem. Ind.* **2006**, 20. (c) Kawata, S.; Kawata, Y. *Chem. Rev.* **2000**, *100*, 1777. (d) Yu, Y. L.; Nakano, M.; Ikeda, T. *Nature* **2003**, *425*, 145. (e) *Molecular Switches*; Feringa, B. L., Ed.; Wiley-VCH: Weinheim, Germany, 2001.

(2) (a) Irie, M.; Fukaminato, T.; Sasaki, T.; Tamai, N.; Kawai, T. *Nature* **2002**, *420*, 759. (b) Dulic, D.; van der Molen, S. J.; Kudernac, T.; Jonkman, H. T.; de Jong, J. J. D.; Bowden, T. N.; van Esch, J.; Feringa, B. L.; van Wees, B. J. *Phys. Rev. Lett.* **2003**, *91*, 207402. (c) He, J.; Chen, F.; Liddell, P. A.; Andreasson, J.; Straight, S. D.; Gust, D.; Moore, T. A.; Moore, A. L.; Li, J.; Sankey, O. F.; Lindsay, S. M. *Nanotechnology* **2005**, *16*, 695. (d) Kudernac, T.; van der Molen, S. J.; van Wees, B. J.; Feringa, B. L. *Chem. Commun.* **2006**, 3597. (e) Katsonis, N.; Kudernac, T.; Walko, M.; van der Molen, S. J.; van Wees, B. J.; Feringa, B. L. *Adv. Mater.* **2006**, *18*, 1397. (f) Zhao, L. Y.; Sui, D.; Chai, J.; Wang, Y.; Jiang, S. M. *J. Phys. Chem. B* **2006**, *110*, 24299.

(3) (a) Senier, A.; Shepheard, F. G. *J. Chem. Soc.* **1909**, *95*, 1943. (b) Senier, A.; Shepheard, F. G.; Clarke, R. *J. Chem. Soc.* **1912**, *101*, 1952. (c) Cohen, M. D.; Schmidt, G. M. J.; Flavian, S. *J. Chem. Soc.* **1964**, 2041.

(4) (a) Moustakali-Mavridis, I.; Hadjoudis, E. *Acta Crystallogr., Sect. B: Struct. Sci.* **1978**, *34*, 3709. (b) Hadjoudis, E. *Chemtronics* **1986**, *1*, 58. (c) Hadjoudis, E.; Vittorakis, M.; Moustakali-Mavridis, I. *Tetrahedron* **1987**, *43*, 1345. (d) Hadjoudis, E. In *Photochromism: Molecules and Systems*; Dürr, H., Bouas-Laurent, H., Eds.; Elsevier: Amsterdam, The Netherlands, 1990; p 685. (e) Hadjoudis, E. *Mol. Eng.* **1995**, *5*, 301. (f) Samat, A.; Lokshin, V. In *Organic Photochromic and Thermochromic Compounds*; Crano, J. C., Guglielmetti, R. J., Eds.; Plenum: New York, 1998; Vol. 2, p 415. (g) Hadjoudis, E.; Mavridis, I. M. *Chem. Soc. Rev.* **2004**, *33*, 579. (h) Amimoto, K.; Kawato, T. *J. Photochem. Photobiol., C* **2005**, *6*, 207.

10.1021/cm800093a CCC: $40.75
Published on Web 05/27/2008

and thermochromism are not exclusive in anils,[7] strategies to favor either property have been described.[8]

Besides the absorption change, other characteristics can be followed during the tautomeric reaction: IR and NMR as well as fluorescence or structural modifications.[5a,9–12] These property changes can be studied either to help the fundamental understanding of the reaction or to exploit them in applications.

During the recent decade, there has been an increasing interest on switching nonlinear optical (NLO) properties by an external trigger.[13] Although studies on NLO properties of anils can be found in the literature,[14] only a few take advantage of their switching ability.[15] We synthesized two isomers *N*-(3,5-ditert-butylsalicylidene)-2-aminopyridine (**1**) and *N*-(3,5-ditert-butylsalicylidene)-4-aminopyridine (**2**, Scheme 2). As already published,[16] **2** crystallizes in the noncentrosymmetric $P3_2$ space group and is second-harmonic generation (SHG) active in the bulk state. By combining with photochromism, we demonstrated its ability to modify reversibly second harmonic generation (SHG). **1** crystallizes in the same space group as **2**, but an important difference is its thermochromism: at room temperature, crystals of **1** are orange and change to yellow when cooled down in liquid nitrogen. Structural investigations and spectral and SHG properties in solution and in solid state are described, and the discussions are aimed to correlate structure with physical properties. Also, we report on thermally induced SHG, and analogy with **2** is made whenever possible.

Scheme 2. Formulas of *N*-(3,5-di-tert-Butylsalicylidene)-2-aminopyridine (1) and *N*-(3,5-di-tert-Butylsalicylidene)-4-aminopyridine (2)

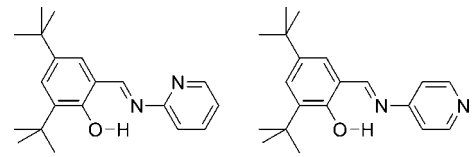

1 **2**

Experimental Section

Synthesis. 1 was synthesized by the same procedure as **2**[16a] by replacing 4-aminopyridine by 2-aminopyridine in the starting materials.

After recrystallization of the crude product in absolute ethanol, orange needles of **1** were obtained (1.3 g, 40%). mp 120 °C. Anal. calcd for $C_{20}H_{26}N_2O$: C, 77.38%; H, 8.44%; N, 8.87%. Found: C, 77.16%; H, 8.57%; N, 8.93%. 1H NMR (DMSO, 300 MHz): δ 1.34 (s, 9H), 1.47 (s, 9H), 7.42 (d, 1H, J 2.2 Hz), 7.51 (d, 1H, J 2.2 Hz), 7.63 (d, 2H, J 5.1 Hz), 7.94 (d, 1H, J 5.1 Hz), 8.57 (d, 1H, J 5.1 Hz), 9.55 (s, 1H), 13.49 (s, 1H). IR: 1616 cm^{-1} (strong, *C*=N), 1576 cm^{-1} (medium, aromatic).

Sample Preparation. Single crystals suitable for X-ray diffraction and for SHG anisotropy measurements were obtained from absolute ethanol. Crystallinity was checked under polarized light microscope. For SHG powder test, these crystals were crushed between two glass blades without any further treatment. X-ray diffraction, SHG anisotropy, and powder measurements were repeated at least twice on crystals collected from the same batch.

To reduce light scattering, other spectroscopic and SHG measurements were made on thin films. They were obtained by melting the previously described crystalline powder between two microscope glass blades ($^1/_{10}$ mm thick) and by cooling down to room temperature. Thickness of these films was estimated to be around 10 μm from weight and density values. Powder X-ray pattern of these semicrystalline samples is compatible with the single crystal's structure.

Crystal Structure Determination. Data for **1** were collected at 120 K and 293 K on an IPDS STOE diffractometer using a graphite-monochromated Mo Kα radiation (λ = 0.71073 Å) and equipped with an Oxford Cryosystem Cooler Device. The final unit cell parameters have been obtained by means of a least-squares refinement performed on a set of 8000 well-measured reflections, and a crystal decay has been monitored during the data collection; no significant fluctuations of intensities have been observed. The

(5) (a) Ogawa, K.; Kasahara, Y.; Ohtani, Y.; Harada, J. *J. Am. Chem. Soc.* **1998**, *120*, 7107. (b) Ogawa, K.; Fujiwara, T. *Chem. Lett.* **1999**, 657. (c) Kabak, M.; Elmali, A.; Elerman, Y. *J. Mol. Struct.* **1999**, *477*, 151. (d) Ogawa, K.; Harada, J.; Tamura, I.; Noda, Y. *Chem. Lett.* **2000**, 528. (e) Chong, J. H.; Sauer, M.; Patrick, B. O.; MacLachlan, M. J. *Org. Lett.* **2003**, *5*, 3823. (f) Chatziefthimiou, S. D.; Lazarou, Y. G.; Hadjoudis, E.; Dziembowska, T.; Mavridis, I. M. *J. Phys. Chem. B* **2006**, *110*, 23701. (g) Rodriguez, M.; Santillan, R.; Lopez, Y.; Farfan, N.; Barba, V.; Nakatani, K.; Baez, E. V. G.; Padilla-Martinez, I. I. *Supramol. Chem.* **2007**, *19*, 641.

(6) (a) Ledbetter, J. W. *J. Phys. Chem.* **1966**, *70*, 2245. (b) Nakagaki, R.; Kobayashi, T.; Nakamura, J.; Nagakura, S. *Bull. Chem. Soc. Jpn.* **1977**, *50*, 1909. (c) Barbara, P. F.; Rentzepis, P. M.; Brus, L. E. *J. Am. Chem. Soc.* **1980**, *102*, 2786. (d) Mitra, S.; Tamai, N. *Phys. Chem. Chem. Phys.* **2003**, *5*, 4647. (e) Ziolek, M.; Kubicki, J.; Maciejewski, A.; Naskrecki, R.; Grabowska, A. *Phys. Chem. Chem. Phys.* **2004**, *6*, 4682. (f) Ohshima, A.; Momotake, A.; Arai, T. *J. Photochem. Photobiol., A* **2004**, *162*, 473.

(7) (a) Fujiwara, T.; Harada, J.; Ogawa, K. *J. Phys. Chem. B* **2004**, *108*, 4035. (b) Harada, J.; Fujiwara, T.; Ogawa, K. *J. Am. Chem. Soc.* **2007**, *129*, 16216.

(8) (a) Kawato, T.; Koyama, H.; Kanatomi, H.; Isshiki, M. *J. Photochem.* **1985**, *28*, 103. (b) Kawato, T.; Koyama, H.; Kanatomi, H.; Tagawa, H.; Iga, K. *J. Photochem. Photobiol., A* **1994**, *78*, 71.

(9) (a) Lewis, J. W.; Sandorfy, C. *Can. J. Chem.* **1982**, *60*, 1738. (b) Carles, M.; Eloy, D.; Pujol, L.; Bodot, H. *J. Mol. Struct.* **1987**, *156*, 43. (c) Turbeville, W.; Dutta, P. K. *J. Phys. Chem.* **1990**, *94*, 4060. (d) Yuzawa, T.; Takahashi, H.; Hamaguchi, H. *Chem. Phys. Lett.* **1993**, *202*, 221. (e) Kaneda, K.; Sato, S.; Hamaguchi, H.; Arai, T. *Bull. Chem. Soc. Jpn.* **2004**, *77*, 1529. (f) Filarowski, A.; Koll, A.; Karpfen, A.; Wolschann, P. *Chem. Phys.* **2004**, *297*, 323.

(10) (a) Sitkowski, J.; Stefaniak, L.; Wawer, I.; Kaczmarek, L.; Webb, G. A. *Solid State Nucl. Magn. Reson.* **1996**, *7*, 83. (b) Alarcon, S. H.; Olivieri, A. C.; Nordon, A.; Harris, R. K. *J. Chem. Soc., Perkin Trans. 2* **1996**, 2293. (c) Kamienski, B.; Schilf, W.; Dziembowska, T.; Rozwadowski, Z.; Szady-Chelmieniecka, A. *Solid State Nucl. Magn. Reson.* **2000**, *16*, 285. (d) Filarowski, A.; Koll, A.; Rospenk, M.; Krol-Starzomska, I.; Hansen, P. E. *J. Phys. Chem. A* **2005**, *109*, 4464.

(11) (a) Cohen, M. D.; Flavian, S. *J. Chem. Soc.* **1967**, 334. (b) Sitkowski, J.; Stefaniak, L.; Wawer, I.; Kaczmarek, L.; Webb, G. A. *Solid State Nucl. Magn. Reson.* **1996**, *7*, 83.

(12) Harada, J.; Uekusa, H.; Ohashi, Y. *J. Am. Chem. Soc.* **1999**, *121*, 5809.

(13) (a) Coe, B. J. *Chem. Eur. J.* **1999**, *5*, 2464. (b) Asselberghs, I.; Clays, K.; Persoons, A.; Ward, M. D.; McCleverty, J. *J. Mater. Chem.* **2004**, *14*, 2831. (c) Sanguinet, L.; Pozzo, J. L.; Rodriguez, V.; Adamietz, F.; Castet, F.; Ducasse, L.; Champagne, B. *J. Phys. Chem. B* **2005**, *109*, 11139.

(14) (a) Palazzotto, M. C. Minnesota Mining and Manufacturing Company. U.S. Patent 4,733,109, March 22, 1988. (b) Bhat, K.; Chang, K. J.; Aggarwal, M. D.; Wang, W. S.; Penn, B. G.; Frazier, D. O. *Mater. Chem. Phys.* **1996**, *44*, 261. (c) Zhang, Y.; Zhao, C. Y.; Fang, W. H.; You, X. Z. *Theor. Chem. Acc.* **1997**, *96*, 129. (d) Bhat, K.; Choi, J.; McCall, S. D.; Aggarwal, M. D.; Cardelino, B. H.; Moore, C. E.; Penn, B. G.; Frazier, D. O.; Sanghadasa, M.; Barr, T. A.; Laxmeshwar, N. B. *Comput. Mater. Sci.* **1997**, *8*, 309.

(15) (a) Nakatani, K.; Delaire, J. A. *Chem. Mater.* **1997**, *9*, 2682. (b) Poineau, F.; Nakatani, K.; Delaire, J. A. *Mol. Cryst. Liq. Cryst.* **2000**, *344*, 89.

(16) (a) Sliwa, M.; Letard, S.; Malfant, I.; Nierlich, M.; Lacroix, P. G.; Asahi, T.; Masuhara, H.; Yu, P.; Nakatani, K. *Chem. Mater.* **2005**, *17*, 4727. (b) Sliwa, M.; Nakatani, K.; Asahi, T.; Lacroix, P. G.; Pansu, R. B.; Masuhara, H. *Chem. Phys. Lett.* **2007**, *437*, 212.

structures have been solved by Direct Methods using SIR 92[17] and have been refined by means of least-squares procedures on an F^2 with the aid of the program SHELXL97[18] included in the software package WinGX version 1.63.[19] The atomic Scattering Factors were taken from the International Tables for X-Ray Crystallography.[20] All hydrogen atoms were located on a difference Fourier map and were refined by using a riding model. All non-hydrogen atoms were anisotropically refined. A twinning problem was successfully treated with the aid of twinRotMat program of Platon (ROTAX).[21] Two systems were isolated (BASF: 0.35/0.65) with 3410 overlapped *hkl* and a transformation matrix of (−1 −1 0/ 0 1 0/0 0 −1).

Drawing of molecules is performed with the program ORTEP32[19,22] with 50% probability displacement ellipsoids for non-hydrogen atoms.

Absorption Spectra. UV−vis absorption spectra of solutions and polycrystalline thin films were recorded on a Varian Cary 5 spectrometer. References for solutions were pure solvents (spectrometric grade). For low-temperature measurements, polycrystalline thin films were placed in a liquid nitrogen cryostat equipped with quartz windows (Oxford Instruments).

Molecular-Scale NLO Property and Dipole Moment (Measurements in Solution). The product of the dipole moment (μ) by the molecular quadratic hyperpolarizability (β) was determined by electric field induced second harmonic (EFISH).[16a,23] The 1064 nm beam of a nanosecond Nd:YAG pulsed laser and the Raman shifted 1907 nm beam were used as the fundamental beams. All experiments were performed in spectrometric grade dioxane. Solutions of MNA (2-methyl-4-nitroaniline, $\mu\cdot\beta = 71 \times 10^{-48}$ esu at 1907 nm and 125×10^{-48} esu at 1064 nm) served as a reference. $\mu\cdot\beta$ values were deduced from the slope ratios between **1** and MNA of the third-order susceptibility of the solution, Γ, versus concentration plots (eqs 1 and 2).

$$\Gamma = A\frac{(I_{2\omega})^{1/2}}{l} \tag{1}$$

$$\Gamma = \Gamma_0 + N_A c f^0 (f^\omega)^2 f^{2\omega}\left[\gamma + \frac{\mu\cdot\beta}{5kT}\right] \tag{2}$$

$I_{2\omega}$ and l are, respectively, the maximum intensity and the period of the Maker fringes, A is an instrument constant, and Γ_0 is the third-order susceptibility of the pure solvent. N_A is Avogadro's number, c is the concentration of the photochrome, f^0, f^ω, and $f^{2\omega}$ are the local field factors (at the frequency written in superscript), γ is the molecular third-order hyperpolarizability, k is the Boltzmann's constant, and T is the temperature. We assumed that the local field factors were the same for the solvent and the solute and that the contribution of γ to Γ was negligible. Under these assumptions, the slope of the Γ versus c plot gives the $\mu\cdot\beta$ value of the solute.

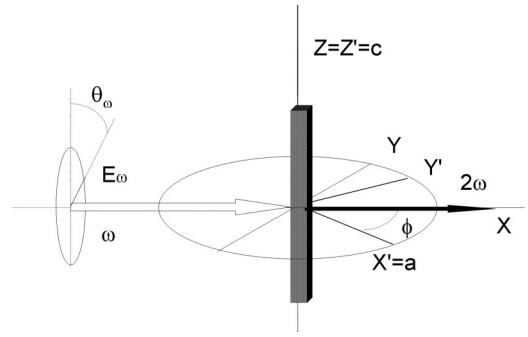

Figure 1. Geometry around the single crystal of **1** for SHG polarization measurements. (X, Y, Z) is the laboratory's axes system, whereas (X', Y', Z') is related to the single crystal.

Dielectric constant and refractive index were measured, respectively, on a dipole meter (WTW) and on an Abbe Refractometer (Carl Zeiss), and μ was determined by following Guggenheim's method.[24]

Material's NLO Properties (Measurements in Solid State). For SHG powder tests, the laser setup described in the previous section was used. The SHG arising from powder samples was compared to that of urea.[25]

Temperature-dependent measurements were made on polycrystalline thin films that were placed in a liquid nitrogen cryostat equipped with quartz windows (Oxford Instruments).

SHG anisotropy was measured on an inverted microscope.[16b] At normal incidence, the fundamental beam of a Ti:sapphire laser (990 nm, 1.3 ps fwhm, 81.2 MHz, 5 mJ pulse^{-1}) was focused on a single crystal (probe volume of a few μm^3), the transmitted light along the X-axis (Figure 1) was collected through a monochromator, and a Glan prism was used to select either the Y- or Z-polarized SHG. Experimental data were corrected by a reference signal. A Fresnel rotator allowed us to rotate θ_ω, the polarization angle between the Z-axis and the fundamental beam's polarization. In the (X', Y', Z') Cartesian axes related to the single crystal, X' and Z' are, respectively, parallel to the crystallographic a- and c-axis, and Y' is in the crystallographic (a, b) plane. The easily recognizable crystallographic axis c of the needle-shaped single crystal was oriented along the Z-axis. Hence, c, Z', and Z are parallel. ϕ was defined as the angle between X and X'.

Theoretical Calculations. The all-valence INDO (intermediate neglect of differential overlap) formalism[26] in connection with the sum over state (SOS) formalism was employed for the calculation of the electronic spectra and the molecular hyperpolarizabilities.[27] In the present approach, the monoexcited configuration interaction (CIS) approximation was employed to describe the excited states. The lowest 100 energy transitions were chosen to undergo CI mixing. All calculations were performed using the INDO/1 Hamiltonian incorporated in the commercially available software package ZINDO.[28]

Results and Discussion

Structure. The X-ray diffraction measurements were performed at 120 K, where the crystals are yellow. Data show

(17) Altomare, A.; Cascarano, G.; Giacovazzo, C.; Guagliardi, A. *J. Appl. Crystallogr.* **1993**, *26*, 343.
(18) Sheldrick, G. M. *SHELX97 [Includes SHELXS97, SHELXL97, CIFTAB] - Programs for Crystal Structure Analysis*, Release 97-2; Institüt für Anorganische Chemie der Universität, Göttingen, Germany, 1998.
(19) Farrugia, L. *J. Appl. Crystallogr.* **1999**, *32*, 837.
(20) *International Tables for X-Ray Crystallography*; Kynoch Press: Birmingham, U.K., 1974; Vol. IV.
(21) (a) Spek, A. L. *J. Appl. Crystallogr.* **2003**, *36*, 7. (b) Cooper, R. I.; Gould, R. O.; Parsons, S.; Watkin, D. J. *J. Appl. Crystallogr.* **2002**, *35*, 168.
(22) Farrugia, L. *J. Appl. Crystallogr.* **1997**, *30*, 565.
(23) (a) Bosshard, C.; Knopfle, G.; Pretre, P.; Gunter, P. *J. Appl. Phys.* **1992**, *71*, 1594. (b) Maltey, I.; Delaire, J. A.; Nakatani, K.; Wang, P. F.; Shi, X. Y.; Wu, S. K. *Adv. Mater. Opt. Electron.* **1996**, *6*, 233. (c) Liu, C. S.; Glaser, R.; Sharp, P.; Kauffman, J. F. *J. Phys. Chem. A* **1997**, *101*, 7176.
(24) (a) Guggenheim, E. A. *Trans. Faraday Soc.* **1949**, 714. (b) Janini, G. M.; Katrib, A. H. *J. Chem. Educ.* **1983**, *60*, 1087. (c) Chen, G. S.; Liu, C. S.; Glaser, R.; Kauffman, J. F. *Chem. Commun.* **1996**, 1719.
(25) Kurtz, S. K.; Perry, T. T. *J. Appl. Phys.* **1968**, *39*, 3798.
(26) Pople, J. A.; Beveridge, D. L.; Dobosh, P. A. *J. Chem. Phys.* **1967**, *47*, 2026. (b) Zerner, M. C.; Loew, G. H.; Kirchner, R. F.; Mueller-westerhoff, U. T. *J. Am. Chem. Soc.* **1980**, *102*, 589. (c) Anderson, W. P.; Edwards, W. D.; Zerner, M. C. *Inorg. Chem.* **1986**, *25*, 2728.
(27) Ward, J. F. *Rev. Mod. Phys.* **1965**, *37*, 1.
(28) *ZINDO*, release 96.0; Molecular Simulations Inc., Cambridge, U.K., 1996.

Table 1. Crystal Data and Structure Refinement for 1 at 120 K[a]

	1
empirical formula	$C_{20}H_{26}N_2O$
formula weight	310.43
T/K	120
crystal system	trigonal
space group	$P3_2$
a/Å	15.599(5)
b/Å	15.599(5)
c/Å	6.246(5)
α/°	90
β/°	90
γ/°	120
volume/Å^3	1316(1)
Z	3
ρ_{calc}/g cm^{-3}	1.175
reflections collected	11314
independent reflections	3410
R(int)	0.4019[b]
R_1 [$I > 2\sigma(I)$]	0.0356
wR_2 [$I > 2\sigma(I)$]	0.0761

[a] See also cif file, Supporting Information. [b] Value before treatment of the twinning problem (see Experimental Section).

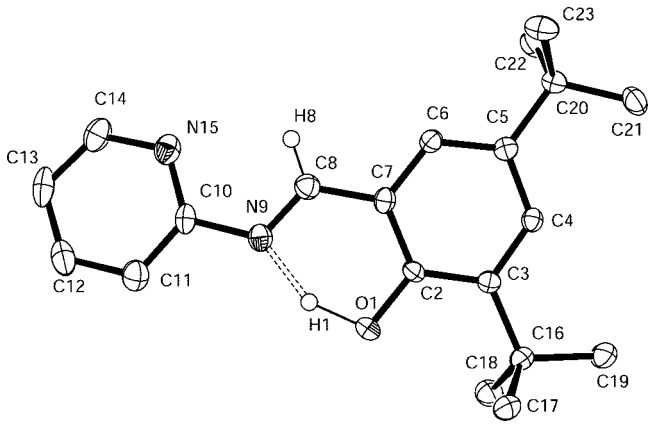

Figure 2. ORTEP view of **1** showing 50% probability displacement ellipsoids. H atoms except H(1) and H(8) are omitted for clarity.

that **1** is in the enol form at this temperature (Table 1, Figure 2).

The overall structure of the molecule is almost planar. Besides the two six-membered rings, two pseudorings exist. The first one (C(2)−O(1)−H(1)···N(9)−C(8)−C(7)) arises from the usual close contact which links the hydroxy group of the enol function to the nitrogen atom of the imine function with a H(1)···N(9) distance of 1.480(4) Å and is responsible for the usual enol−keto tautomerism. The other one (2.312(3) Å) involves the imine hydrogen, H(8), and the pyridine nitrogen, N(15), and favors the quasi-planar structure of the *N*-salicylidene-aminopyridine backbone: the angle between the pyridine ring and the benzene ring bearing the enol function is only $\delta = 6.8(2)°$. This structural feature is typical of thermochromic compounds, since it is well established that low δ angle values lead to thermochromism whereas high values lead to photochromism. In our case, the position of the pyridine nitrogen plays a crucial role on the properties:[4a] **1** is thermochromic, whereas **2** is photochromic. In the latter, nitrogen occupies the 4-position, and hence, no intramolecular interaction with hydrogen atom is possible, and the molecule's backbone is much more distorted (δ = 41.8(1)°).[16a]

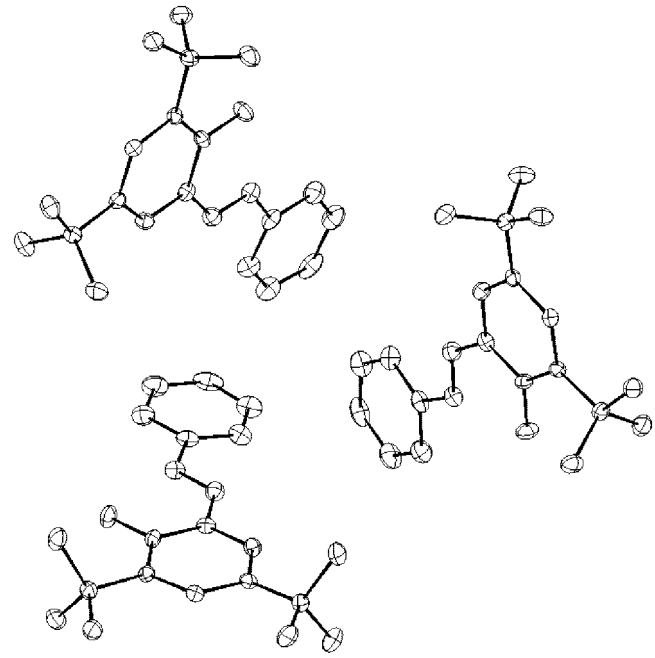

Figure 3. Unit cell of **1**, view along the *c* axis. H atoms are omitted for clarity.

In the lattice, one molecule is deduced from the other by a rotation of 120° in the *ab*-plane and a translation of $^1/_3$ in the *c*-direction, which is a 3-fold axis. The molecules make a helix around the *c*-axis in a non-centrosymmetric fashion (Figure 3). The resulting space group is $P3_2$, just like the photochromic isomer **2**, which provides bulk crystalline SHG activity in both cases. This point will be discussed in the NLO properties section.

According to previous studies,[3,4] the color at room temperature is attributed to the presence of the keto form. X-ray diffraction data at room temperature did not show any noticeable difference from those at 120 K. In fact, in such enol−keto mixtures, the resulting structure is a superposition of the two isomers, which is difficult to solve.[5a,b] In the present case, C(7)−C(8) bond shortens and C(8)−N(9) bond lengthens upon heating, which is compatible with an enol-to-keto conversion. However, these temperature-induced distance changes are ∼0.01 Å between 120 K and room temperature and cannot be considered as significant. A low enol-to-keto conversion is a possible reason for this absence of clear structural difference.

Absorption Spectra. Whatever the solvent, the solution of **1** is slightly yellow at room temperature. The absorption spectrum has two maxima in the 300−400 nm domain (Figure 4) separated by ca. 50 nm, and both show a slightly negative solvatochromism (Table 2). **2** also has two absorption bands in the same region; however, the main difference from **1** is the slightly positive solvatochromism of the lower energy band. In the solid state, high absorption combined with light scattering does not allow to observe the previously mentioned UV absorption bands in transmission mode. However, diffuse reflectance spectroscopy clearly showed the two bands observed in solution (Table 2, see Supporting Information).[29]

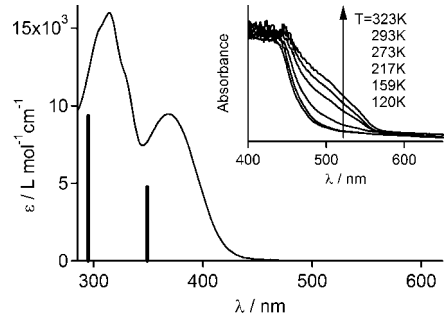

Figure 4. Absorption spectra of **1** in $CHCl_3$. ε is the molar absorption coefficient. The bar graph shows the ZINDO calculated transitions with heights proportional to the oscillator strength. Inset: absorption spectra of a polycrystalline thin film at various temperatures between 120 K and 323 K.

Table 2. Absorption Bands of 1

solvent	ε_r	μ /D	λ_1 /nm	λ_2 /nm
cyclohexane	2.02	0	370	314
toluene	2.38	0.43	369	315
chloroform	4.83	1.15	370	314
ethanol	24.3	1.69	365	312
aceton	20.7	2.82	363	311
acetonitrile	37.5	3.45	362	310
powder			366[29]	309[29]
calculated			349	295

Table 3. Analysis of the ZINDO Computed Data for the Main Transitions of Molecule 1

transitions [a]	1→2	1→4	1→7
λ/nm	349	295	247
$\lvert\vec{\mu}_e\rvert$/Dc	3.36	2.85	4.03
$\lvert\vec{\mu}_e - \vec{\mu}_f\rvert$/D[d]	5.50	0.81	5.54
f[e]	0.29	0.57	0.15
ρ_n[f]	36%	6%	6%
orbitals	61→62[b]	60→62	61→62 60→62 61→66
character	phenol→C=N + pyridine	phenol→pyridine + C=N	phenol→C=N

[a] Transitions 1→3, 1→5, and 1→6 have negligible oscillator strengths compared to 1→2, 1→4, and 1→7. [b] Orbitals 61 and 62 are, respectively, HOMO and LUMO. [c] $\lvert\vec{\mu}_e\rvert$: dipole moment of the excited state (ground-state dipole moment: $\mu_0 = 3.42$ D). [d] $\lvert\vec{\mu}_e - \vec{\mu}_f\rvert$: dipole moment change between fundamental and excited states. [e] f: oscillator strength. [f] ρ_n: contribution of the transition to NLO properties calculated according to the following formula: $\rho_n = (f_n\Delta\mu_n/E_n^3)\ [E_n^4/(E_n^2 - E_\omega^2)(E_n^2 - E_{2\omega}^2)]/\Sigma n = 1^{100} f_n\Delta\mu_n/E_n^3\ [E_n^4/(E_n^2 - E_\omega^2)(E_n^2 - E_{2\omega}^2)]$ where E_n, E_ω, and $E_{2\omega}$ are, respectively, the energy of the transition, the fundamental, and the second-harmonic waves.

ZINDO calculations provide a rationale for these results. The data gathered in Table 3 give absorption bands blue-shifted from experimental results with maxima located at 349 nm (transition 1→2, highest occupied molecular orbital (HOMO)→lowest unoccupied molecular orbital (LUMO)) and 295 nm (transition 1→4, HOMO-1→LUMO) corresponding, respectively, to λ_1 and λ_2. However, the agreement between calculated and experimental values of the bands' relative positions and oscillator strengths is satisfactory. As expected, the phenol group acts as a donor moiety. Moreover, according to calculations, the ground state ($\mu_0 = 3.42$ D) is slightly more polar than the excited states of these transitions, which rationalizes the weakly negative solvatochromism observed experimentally. The role played by these bands in the NLO properties will be discussed in a later section.

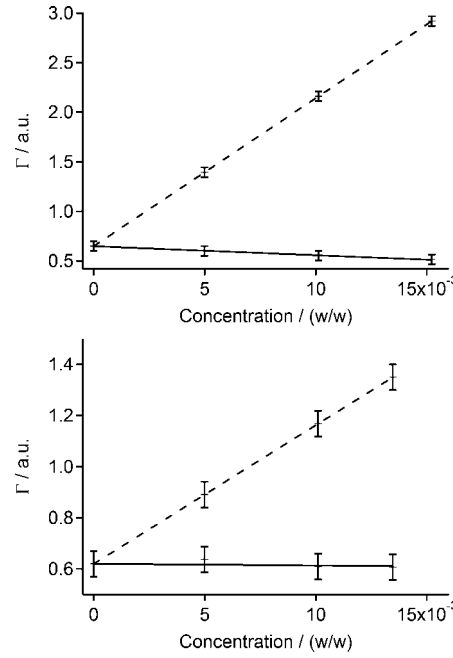

Figure 5. EFISH measurements. Nonlinear function Γ (see eq2) vs concentration curves at 1064 nm (top) and at 1907 nm (bottom). Concentration is expressed in **1** vs solvent mass fraction (w/w). $\mu\cdot\beta$ values are obtained from comparison of the slope between **1** (full line) and MNA (dashed line).

While changing the temperature, a significant absorption spectrum modification is observed on thin films. Upon heating from 120 to 322 K, the absorbance increases in the 450−550 nm region (Figure 4). A spectral broadening cannot be the only explanation, and the appearance of an additional band around 470 nm, typical of the orange keto form, seems to be the main contribution to this spectral change (Figure 4). Another signature of the enol−keto mixture at room temperature is the presence of a dual fluorescence band, which cannot be seen in **2** (see Supporting Information). The keto isomer is absent from solution at room temperature and can be seen only by transient methods.[29] Such a feature is usual for anils whether they are photochromic or thermochromic in the solid state.

Molecular NLO Properties. Second-order NLO properties were determined by the EFISH method in dioxane. Γ values (see Experimental Section, eqs 1 and 2), which are directly connected to the SHG intensity, were determined at 1064 and 1907 nm for solutions of **1** with different concentrations. $\mu\cdot\beta$ corresponds to the slope in Γ versus concentration plots (Figure 5). $\mu\cdot\beta$ was found to be equal to $-(16 \pm 6) \times 10^{-48}$ esu at 1064 nm. The experimental value of μ is rather different from the calculated one (Table 4). The low value of μ may be the cause of such a discrepancy, but another possible reason is the structural difference between the solution and the solid state, since the calculations are based on X-ray data. Considering the experimental value of μ (1.9 D or 1.9×10^{-18} esu), β_μ (β along the dipole moment's direction) is $-(8 \pm 3) \times 10^{-30}$ esu at 1064 nm. At 1907 nm, solutions of **1** have Γ values,

(29) Sliwa, M.; Nakatani, K.; Métivier, R.; Asahi, T.; Masuhara, H. submitted.
(30) Shen, Y. R. *The Principle of Nonlinear Optics*; Wiley: New York, 2002.

Table 4. Experimental and Theoretical Dipole Moment (μ) and Quadratic Hyperpolarizability (β) Values

		β_μ /10^{-30} esu[a]	
	μ /D	1907 nm	1064 nm
exp.	1.9	0 to −5	-8 ± 3
theor.	3.4	−4.3	−5.6

[a] β_μ represents the projection of β along μ's direction.

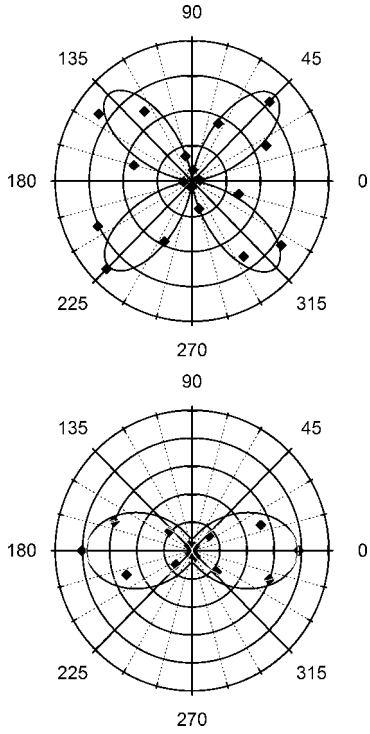

Figure 6. *Y*-polarized (left) and *Z*-polarized (right) SHG intensity of a single crystal of **1** (radius) as a function of the fundamental beam polarization (θ_ω, angle). Experimental data (■) and calculated curves (full line).

which do not differ much from the pure solvent. Hence, we can only deduce that -10×10^{-48} esu $< \mu \cdot \beta < 0$ and that β_μ is negative with a very low value (between 0 and -5×10^{-30} esu).

The relatively low values of μ and β are rather expected for this compound, which bears no strong acceptor or donor group. This is also the case for **2**[16a] and for other anil compounds reported so far.[14b,c] There is a quite good match between experimental and theoretical β_μ values (Table 4). According to ZINDO calculations, 1→2, 1→4, and 1→7 transitions are the most important transitions in terms of contribution to the NLO properties (Table 3). In all transitions, the phenol moiety acts as an electron donor. The negative β_μ values are consistent with the negative solvatochromism mentioned above, and both originate from the higher polarity of the ground state compared to the excited states for the first two transitions. Although this effect is very weak, it was nevertheless confirmed by ZINDO calculations.

Macroscopic NLO Properties. *1. SHG Measurements by Powder Test and Polarization Dependence on a Single Crystal.* Powder samples of **1** generate an SHG signal of 2 compared to urea at 1907 nm. Despite its rather poor molecular NLO properties, the non-centrosymmetric helicoidal structure allows **1** to have a reasonable SHG intensity in its crystalline state. This is also the case for **2**, which has a similar molecular and bulk structure (SHG equal to 3 times urea under the same conditions).[16a]

Table 5. NLO Coefficient Components d′ Involved in Eqs 3 and 4 [a]

contracted indices (*IJ*)	full indices (*IJK*)	NLO coefficients (in au)
11	*X′X′X′*	−29
15	*X′Z′X′*	417
22	*Y′Y′Y′*	255
31	*Z′X′X′*	279
33	*Z′Z′Z′*	820

[a] Calculated by ZINDO method at 990 nm expressed in the crystal's Cartesian axes system (*X′*, *Y′*, *Z′*) (1 au = 8.64×10^{-33} cm^5/esu).

Polarization-dependent SHG measurements were performed on a single crystal.[16b] The incident polarization angle (θ_ω) was rotated in the *YZ* plane, and the *Y*- and *Z*-polarized SHG intensities were measured (Figure 6). The polar plot of the *Y*-polarized SHG has a cloverleaf-shaped curve: the value is minimal for incident beam's polarization parallel to *Y*- and *Z*-axes and is maximal between the axes where $\theta_\omega \equiv 45°$ (mod 90°). In *Z*-polarization, the signal is maximal at $\theta_\omega \equiv 0°$ (mod 180°) and almost vanishes at $\theta_\omega \equiv 90°$ (mod 180°).

2. Calculations of the Polarized SHG on a Crystal. Since we worked at normal incidence and on a small sample volume (see Experimental Section), we neglected the influence of the refractive index and the phase mismatch. Under such assumptions, the SHG intensity polarized along *Y* and *Z*, respectively, is directly proportional to $|P_Y|^2$ and $|P_Z|^2$, the *Y*- and *Z*-components of P_{NL}, expressed as follows:[30]

$$P_Y = E_\omega^2\{[d_{11}'(3\cos^2\varphi\sin\varphi - \sin^3\varphi) + d_{22}'(\cos^3\varphi - 3\sin^2\varphi\cos\varphi)]\sin^2\theta_\omega + 2d_{15}'\cos\theta_\omega\sin\theta_\omega\} \quad (3)$$

$$P_Z = E_\omega^2\{d_{31}'\sin^2\theta_\omega + d_{33}'\cos^2\theta_\omega\} \quad (4)$$

E_ω and θ_ω are, respectively, the amplitude and the polarization angle of the fundamental beam. ϕ is the angle between the (*X*, *Y*, *Z*) and (*X′*, *Y′*, *Z′*) axes as defined in Figure 1.

d'_{IJ} are the components of the second-order NLO coefficients tensor in the (*X′*, *Y′*, *Z′*) coordinates system. These were calculated on one unit cell of **1**, since we can consider that NLO coefficients of the unit cell are directly proportional to those of the macroscopic single crystal.[31] Atomic coordinates determined from X-ray diffraction were used. The results of the calculations are compatible with the trigonal symmetry of the crystal (see Supporting Information). The components involved in the expressions of SHG intensity are gathered in Table 5. The most important ones are d'_{15} and d'_{33}, respectively, for *Y*- and *Z*-polarizations.

For *Y*-polarized SHG, the experimental data were fit with the calculated d'_{IJ} values and $\phi \equiv 48°$ (mod 60°). There is a quite good fit of the experimental values to the theoretical ones, and the cloverleaf shape is modeled by eq 3, where the importance of d'_{15} at incident angles of $\theta_\omega \equiv 45°$ (mod 90°) appears clearly.

For *Z*-polarization, from calculated d'_{31} and d'_{33} values and by means of eq 4, we can deduce that the SHG intensity maximum and minimum are, respectively, at $\theta_\omega = 0°$ and

(31) Zhu, X. L.; You, X. Z.; Zhong, Y.; Yu, Z.; Guo, S. L. *Chem. Phys.* **2000**, *253*, 241.

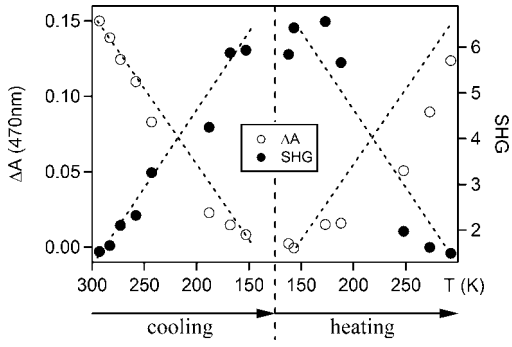

Figure 7. Absorption change at 470 nm (ΔA, ○) and SHG intensity (●) variation upon a cooling−heating cycle. Dashed lines are only to guide the eyes.

90°. In Figure 6, we represented the polar plot with calculated d'_{31} and d'_{33} values. The calculated shape matches the experimental data.

The calculations are based on crystallographic data at 120 K where only the enol form exists, whereas the experiments are performed at room temperature where a slight amount of keto is present in the crystal. Despite this, calculations fit the experimental data rather well. The role of the keto isomer on the NLO properties of the sample will be discussed in the next section.

Thermochromism and Thermally Induced SHG Variation. As already described in a previous section, a strong color change occurs when a solid sample of **1** is cooled in liquid nitrogen. A concomitant variation of the SHG intensity occurs (Figure 7), and the value at 120 K is 4 times as high as at room temperature. The initial absorbance and SHG values are recovered after heating the sample back up to room temperature. On the same temperature range, such a change was not observed for the photochromic (but nonthermochromic) **2**.

As it is the case of other solid-state anils studied so far,[16,32] evolving the keto isomer induces a decrease of SHG. Since the pure keto compound cannot be obtained, it is difficult to determine the relative keto versus enol NLO properties. Theoretical calculations show that it strongly depends on the substituents.[33] Several possible explanations of the SHG decrease upon the appearance of the keto form are (1) lower molecular NLO properties of the keto form compared to the enol, (2) an orientational change of the NLO components during the isomerization, and (3) a large refractive index change between the enol and the keto forms, which may indirectly affect the SHG intensity.

Conclusion

In anils, tautomerism occurs rather easily by means of temperature or light. This duality is very well illustrated by comparing **1** with its isomer **2**. Both do not have a push−pull structure but exhibit SHG, since they both form a chiral helix structure and crystallize in the $P3_2$ space group. Their polarization dependence of SHG is similar. However, by changing the position of one atom, the molecular geometry is totally different, leading to thermochromism in one case and to photochromism in the other. **1** is a thermoresponsive and **2** a photoresponsive NLO material. Further comparative work on this molecule pair is currently in progress, for example, on the reaction process. Also, investigations for higher contrast of signals are performed to reach a "1/0" switching system.

It is particularly interesting to note that a very small structural change induces important effects on absorption and SHG intensity, which are reversible. This family of compounds is very promising for applications as switches driven by an external trigger such as heat or light.

Acknowledgment. The authors thank Ms. Laure Vendier, Mr. Jean-Jacques Vachon, and Mr. Arnaud Brosseau for technical assistance in sample characterization, X-ray diffraction measurements, and SHG measurements under the confocal microscope. This work was funded by the "ACI Physicochimie de la matière complexe" program of the French Ministry of Research.

Supporting Information Available: Absorption, diffuse reflectance, and fluorescence spectra; ZINDO calculation results: NLO coefficients of the crystal of **1** (PDF). X-ray crystallographic data for compound **1** (COF). Deposited data: CCDC 655341. This material and is available free of charge via the Internet at http://pubs.acs.org.

CM800093A

(32) Spangenberg, A.; Sliwa, M.; Métivier, R.; Dagnélie, R.; Nakatani, K.; Pansu, R.; Malfant, I. *J. Phys. Org. Chem.* **2007**, *20*, 992.

(33) Guillaume, M.; Champagne, B.; Markova, N.; Enchev, V.; Castet, F. *J. Phys. Chem. A* **2007**, *111*, 9914.